

Received 30 May 2024, accepted 8 July 2024, date of publication 1 August 2024, date of current version 3 October 2024.

Digital Object Identifier 10.1109/ACCESS.2024.3436643

RESEARCH ARTICLE

Additive Manufacturing of Nd-Fe-B Permanent Magnets and Their Application in Electrical Machines

JULAN WU¹, OGUZ KORMAN², MAURO DI NARDO³, (Member, IEEE),
MICHELE DEGANO², (Senior Member, IEEE), CHRIS GERADA², (Senior Member, IEEE),
IAN ASHCROFT⁴, RICHARD J. M. HAGUE⁴, AND NESMA T. ABOULKHAIR^{4,5}

¹Research and Development Group, Cooksongold, B1 3NZ Birmingham, U.K.

²Power Electronics, Machines and Control Group, Faculty of Engineering, University of Nottingham, NG7 2RD Nottingham, U.K.

³Department of Electrical Engineering and Information Technology, Politecnico di Bari, 70126 Bari, Italy

⁴Centre for Additive Manufacturing, Faculty of Engineering, University of Nottingham, NG8 1BB Nottingham, U.K.

⁵Additive Manufacturing Laboratory, Advanced Materials Research Centre (AMRC), Technology Innovation Institute (TII), Abu Dhabi, United Arab Emirates

Corresponding author: Julian Wu (Julan.wu@cooksongold.com)

This work was supported by the INNOVATIVE doctoral program, which was partially funded by the Marie Curie Innovative Training Networks (ITN) action (project number 665468) and partially by the Institute for Aerospace Technology (IAT) at the University of Nottingham.

ABSTRACT Powder Bed Fusion-Laser Beam (PBF-LB), a form of additive manufacturing (AM) for Nd-Fe-B permanent magnets, is attracting substantial interest for its ability to process functional magnetic materials while capitalizing on AM's design flexibility and waste reduction. As the demand for rare-earth magnets declines due to scarcity and high costs, AM emerges as a pivotal player in the future of electrical machines. However, crack formation and delamination during laser-based AM hinder the production of hard magnetic Nd-Fe-B components, compromising part integrity. This paper addresses these challenges by successfully controlling laser scan strategies and presenting an approach to minimize delamination. Resin infiltration is explored as a potential solution to mitigate residual cracking. Optimized scan strategies and resin infiltration enhance the structural integrity of printed magnets, meeting specific application requirements. As a vessel to investigate the proposed approach for the AM of Nd-Fe-B magnets, a Permanent Magnet assisted Synchronous Reluctance motor has been designed using a particular shape of permanent magnets enabled by the AM. Experimental results align with the FE findings, showcasing a 12% increase in average torque using PBF-LB-produced permanent magnets. This indicates that AM's enhanced design freedom, unconventional shapes, and minimal post-processing contribute to improved reliability, efficiency, and overall performance.

INDEX TERMS Additive manufacturing, magnetic properties, Nd-Fe-B permanent magnets, permanent magnet assisted synchronous reluctance (PMaSynRel) motors, powder bed fusion-laser beam (PBF-LB).

I. INTRODUCTION

Nd-Fe-B magnets are widely used in electro-magneto-mechanical devices [1], [2] owing to their high energy density and good magnetic stability [1]. Traditionally, Nd-Fe-B magnets are manufactured using conventional sintering methods and require machining to realize their final geometry and dimensions. Due to manufacturing constraints, the geometries achievable for Nd-Fe-B magnets are usually limited to

rectangular or circular cross-sections. Additive Manufacturing (AM) has previously demonstrated excellent capabilities to manufacture net-shape parts with high degrees of design freedom, eliminating the need for additional machining, thus minimizing material waste. Considering the potential use of topology optimization for next generation electric machines [3], the design freedom of AM applied to permanent magnets has the potential to enable more powerful and efficient devices. Using AM also reduces waste of rare-earth elements due to the possibility of reusing the unfused powder in subsequent builds. This is particularly attractive because

The associate editor coordinating the review of this manuscript and approving it for publication was Chung-Tse Michael Wu.

of the environmental impact of extracting the rare-earth elements and their availability [4]. Permanent magnet motors are used in e-mobility and aerospace applications requiring high efficiency, performance, and power density [5]. Therefore, adopting AM to produce Nd-Fe-B magnets is a key enabler for improving a motor's performance by means of more complex magnet geometries whilst saving precious resources. Nd-Fe-B magnets have been produced by various AM techniques [6], [7], [8], [9], [10], [11], [12], [13], [14], e.g. extrusion-based methods, electron beam melting (PBF-EB) and powder bed fusion - laser beam (PBF-LB). The magnetic properties of the permanent magnets produced by PBF-LB were found to be superior to those by extrusion-based techniques owing to the higher metallic density produced with this process, and in comparison, to the e-beam produced sample due to the presence of the preferable permanent magnetic phase. Although PBF-LB was shown to produce magnets with comparable properties to conventionally produced isotropic magnets, there still exist some challenges that need to be addressed. Previous studies were mainly focused on optimizing the process parameters (e.g. laser power, scan speed, hatch distance) that are directly related to the magnetic properties of the produced parts [12]. For instance, Bittner et al. [11], [12], reported that remanence was improved from 0.52 T to 0.63 T through tuning the process parameters. Further improvements using this approach were inhibited by the fact that the material started to fail by delamination at excessive energy inputs [12], [13], [15]. Besides process parameters, the integrity of the parts was also affected by the sample's size and geometry [13], which were limited. The brittle material mainly suffered from micro-cracks attributed to thermal and phase transition stresses [13]. As a result, delamination was mainly observed at the corners while cracks were randomly distributed across the whole sample [11], [13]. On one hand, delamination during processing inhibits successful production of magnets with certain geometric designs necessary for specific applications [13]. However, the mechanical properties deteriorated with the presence of the cracks, compromising the performance of the magnets. To better support the notion of the application of this material, minimizing delamination for any geometric design and inhibiting the propagation of cracks are of great importance.

Permanent magnet assisted synchronous reluctance (PMA_{SynRel}) motors present a rotor structure formed by a combination of air barriers (partially filled by PMs) and ferromagnetic iron paths to conduct the flux through the rotor structure, and their torque production is given by two components: the reluctance and the permanent magnets. PMA_{SynRel} motors are more cost-effective with lower permanent magnet content compared to internal and surface permanent magnet machines, in which torque production occurs mostly owing to the presence of magnets. The introduction of permanent magnets to pure reluctance machines can yield a significant improvement in terms of torque and power [16]. To create rotor slots to allow the insertion of

conventional rectangular shaped permanent magnets, it is a common practice to modify the optimal shape of the flux barriers described by the Joukowski function [17]. This choice is clearly not preferred and limits the performance's improvement. Indeed, shaping the permanent magnets to fully fill the optimal shaped flux barriers is expected to lead to improved performance.

In this study, in-process scan strategy during PBF-LB processing and post-process resin infiltration were studied to produce curved permanent magnets for a PMA_{SynRel} machine. The performance of the machine are analyzed by finite element analysis (FEA), using the measured magnetic characteristics of the magnets. Additionally, the performances of the machine equipped with the as built and resin infiltrated magnets were compared in an experimental setup that measures the induced voltage at no load conditions. Experimental verifications of both the as-printed and resin-infiltrated magnets were conducted and compared with the simulation results.

II. PERMANENT MAGNET ASSISTED SYNCHRONOUS RELUCTANCE MACHINE

The exploitation of AM techniques to produce permanent magnets that can be integrated into an optimal SynRel structure, with shapes that would be otherwise challenging to achieve, is proposed, and assessed. With the aim of testing the performance of PBF-LB Nd-Fe-B magnets, a 4-poles 24 slots SynRel machine prototype was considered as a case study. Its design was optimized to operate without permanent magnets, however, as discussed earlier, the permanent magnets' insertion can significantly benefit the torque generation. The general dimensions of the baseline machine are given in FIGURE 1 and Table 1. For simplicity, and to minimize the number of permanent magnets to insert into the rotor, only the innermost air layers were selected for magnet insertion (FIGURE 1 (b)). A magnetization jig was printed with Polyamide (PLA) filament using a fused deposition modelling (FDM) Ultimaker 3D printer (Ultimaker B.V., Netherlands), to hold the produced magnets for magnetization in a specific orientation using a MAGSYS magnetizer (MAGSYS magnet system, Germany). The magnets were inserted into the air barriers of the rotor (as shown in FIGURE 1 (c)) to enhance the torque and power production.

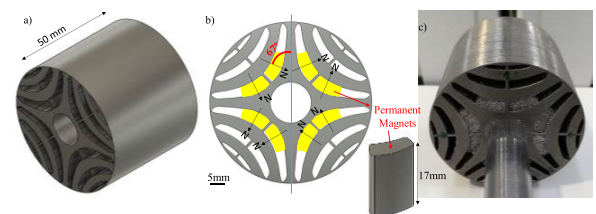


FIGURE 1. Schematic of a) the geometry of the laminated rotor and b) the magnetization orientation and dimensions of the PBF-LB Nd-Fe-B permanent magnets to be inserted into the laminated rotor; c) photograph of the PMA_{SynRel} motor with the inserted as-built magnets.

TABLE 1. General dimensions of the PMaSynRel machine.

	Value	Unit
Stator outer diameter	102	[mm]
Rotor outer diameter	59.4	[mm]
Air gap length	0.3	[mm]
Lamination stack length	50	[mm]
Stator and Rotor Lamination Material	M470	

III. PRODUCTION OF THE ND-FE-B PERMANENT MAGNETS USING PBF-LB

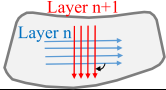
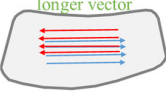
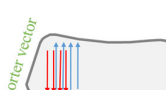
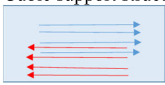
Pre-alloyed gas atomized Nd-Fe-B powder (MQP-S-11-9-20001) with a chemical composition of Nd_{7.5}Pr_{0.7}Zr_{2.6}Ti₂.5Co_{2.5}Fe₇₅B_{8.8} [18] was supplied by Magnequench (Germany). The powder was sieved using a 75 μm sieve and dried at 65 °C for 1h prior to PBF-LB processing. The specimens were manufactured using a Renishaw AM125 system (Renishaw, United Kingdom), equipped with an yttrium fiber continuous wavelength laser with a maximum power of 200W and a spot size of 40 μm operating in a pulsed mode. The feedstock material was kept in sealed bottles before use and the processed samples were stored in vacuumed bags to avoid oxidation. The parts were manufactured under argon atmosphere with an oxygen level below 500 ppm, on a mild steel build-plate, heated up and maintained at 190 °C during processing (the highest temperature achievable on the system) to reduce the thermal gradient during solidification to minimize the residual stresses and warping.

A. SCAN STRATEGY STUDY ON THE STRUCTURAL INTEGRITY

The employed parameter combination was optimized and published in an earlier study [13], and the main ones are: a layer thickness of 30 μm, a point distance of 65 μm, an exposure time of 72 μs, a hatch distance of 100 μm, and a bi-directional scan strategy with a rotation of 67° between layers. To produce the magnets for insertion in the motor for application assessment, each magnet with the geometry shown in Table 2 (b) was printed on a cubic support structure. The choice of the cubic support structure was based on the material’s physical brittleness. Intricate support structures with thin walls, commonly used in other materials, were not suitable for this material. To provide the fundamental mechanical support for the samples, yet be able to easily remove the supports, parameters resulting in a lower relative density were employed for the latter. The parameter combinations used to process the parts and the supports are displayed in Table 2, resulting in relative densities of 91% and 85%, respectively [13].

Given the peculiarity of this material when it comes to PBF-LB processing, to cope with the geometry of the magnets, three scan strategies were tested with the aim of minimizing delamination during production and improving the structural integrity of the printed parts. Strategies with

TABLE 2. Parameter combinations applied to process the parts and the support structures using the three tested scan strategies.

ID	Scan strategy	Rotation between layers	Parameter combination
a) Part A	 Unidirectional	90°	Layer thickness: 30 μm Hatch distance: 100 μm Laser power: 100 W Point distance: 65 μm Exposure time: 72 μs
b) Part B	 Unidirectional (Perpendicular ar to the long edge)	180°	Layer thickness: 30 μm Hatch distance: 100 μm Laser power: 100 W Point distance: 65 μm Exposure time: 72 μs
c) Part C	 Unidirectional (Perpendicular ar to the short edge)	180°	Layer thickness: 30 μm Hatch distance: 100 μm Laser power: 100 W Point distance: 65 μm Exposure time: 72 μs
Cubic support structure	 Unidirectional	180°	Layer thickness: 30 μm Hatch distance: 100 μm Laser power: 100 W Point distance: 65 μm Exposure time: 55 μs

variations in the scanning directions in a layer and the rotation between layers were designed. These strategies are schematically illustrated in Table 2 and hereafter denoted as A, B, and C. The design of the scan strategies was guided by prior understanding of the formation of the thermal cracks during processing [13]. Based on the temperature gradient mechanism (TGM) applicable to PBF-LB of an iron-based material [40], the part’s geometry (i.e. the cross-section per layer) and time-varying parameters during the process using different scan strategies can influence the local temperature of the parts, resulted in varying thermal gradient and residual stress. This Nd-Fe-B material is prone to delamination at boundaries and sharp corners [13]. Rather than the bi-directional scan strategy used in the previous research [13], a unidirectional one was found to reduce defects at the boundaries and corners of the samples. It was found that the parts produced with the unidirectional scan and 90° of rotation between the layers (“A”) showed best structural integrity without significant surface defects compared to parts “B”, where the layers were rotated by 180° from each other. In the case of the latter, delamination was observed in the extruded region, which was poorly mechanically restrained. This agrees with earlier findings in the literature. The 90° rotation of scan vectors between the layers was reported to be beneficial in reducing the part distortion [42], [43] and enhancing the mechanical properties of the samples owing to lower temperature gradients [44] according to the TGM.

Compared to parts “B”, parts “C” were produced using shorter scan vectors following the shorter edge of the cross-section (as illustrated in Table 2) and showed significantly poorer structural integrity. Parts “C” failed prematurely during the manufacturing process, most possibly due to the higher thermal gradient when processed by shorter scan vectors. Based on the temperature gradient mechanism (TGM) [40], this can be explained as follows: at a fixed scan speed of the laser beam, each point in a scan track will be partially re-melted sooner by the neighboring scan track due to the shorter scan vector and therefore a higher temperature could be reached. Consequently, a higher thermal gradient would generate more residual stresses during cooling, resulting in severe deformation and part distortion.

Parts “A”, “B” and “C” produced using the various scan strategies tested in this study are shown in TABLE 3. The structural integrity of the parts was significantly affected by the scan strategy (scan direction and rotations between the layers). The impact of the thermal stresses arising during the PBF-LB process on the quality of the printed materials is well-established [39], [40], [41]. Both the transient and residual thermal stresses developed in the part are associated with the process parameters and the material’s properties. Compared to other alloys, such as stainless steel, titanium and aluminum alloys [13], the combination of low thermal conductivity and fracture toughness of Nd-Fe-B makes it more prone to cracking during processing and imposes more limitations on the achievable geometries. The material’s low thermal conductivity leads to high thermal gradients, resulting in elevated thermal stresses. Additionally, the material’s low fracture toughness renders it prone to crack propagation during processing.

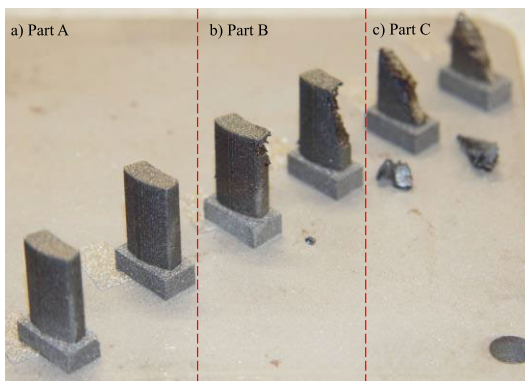


FIGURE 2. Photographs of the produced parts using the scan strategies as shown in a) b) and c) respectively in Table 3. The cubic support structure can be seen under the main part.

B. EFFECT OF RESIN INFILTRATION

Using the optimized scan strategy resulted in the best structural integrity, multiple samples were printed on one build plate to maximize productivity, as shown in FIGURE 3 (a). A sample was also analyzed using X-ray micro-computed tomography (μ CT) using a Xradia 500 Versa X-Ray Micro-

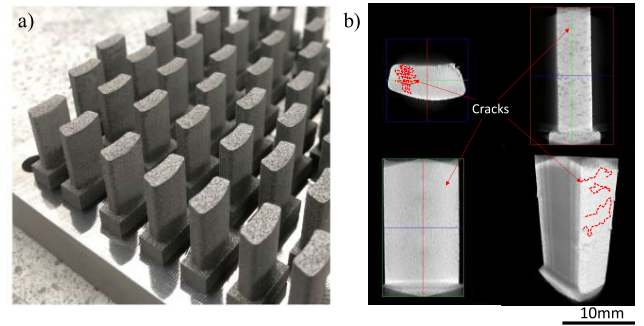


FIGURE 3. a) PBF-LB Nd-Fe-B samples with designed geometric shape printed with the optimized scan strategy and parameter combination to be inserted into the laminated rotor; b) The μ -CT images showing micro-cracks across the parts.

scope (Zeiss, Oberkochen, Germany) using the following setup: accelerating voltage of the X-ray tube source 160 kV, source current 63 μ A, projections 1601, exposure time 24 s, geometric magnification 6.1X and optical magnification 0.4X. The pixel/step size (resolution) was 5.5 μ m. The sample was placed 22 mm away from the X-ray source and 113 mm from the detector. X-ray imaging and volumetric reconstruction were performed using a filtered back projection reconstruction algorithm. Although samples of sufficient structural integrity were produced, micro-cracks were observed across the whole sample in the μ CT scans, as shown in FIGURE 3 (b).

To test whether resin infiltration can be a viable route to address this matter, epoxy resin EpoFix from Struers (Denmark) was infiltrated to the printed samples using the vacuum chamber of the CitoVac vacuum mounting machine (Denmark), which ensures no presence of air for better impregnation of the samples. EpoFix is a low viscosity epoxy system where the resin and hardener are mixed at a volumetric ratio of 15:2, which can cure at room temperature after 12 hours. To demonstrate the infiltration of the resin into the samples, EpoDye from Struers (Denmark) was added to EpoFix, which made it distinguishable under the confocal microscope ZEISS LSM 900 (ZEISS, Germany) equipped with fluorescent light.

The formation of cracks in this material during processing is attributed to the high thermal gradient during cooling and solidification due to the brittle nature of the alloy [13]. The robustness of the as-built samples was weakened by the presence of these interconnected cracks, as can be seen in FIGURE 4 (a). The more significant negative impact of the crack networks and the fragility of the samples was evident during the insertion of the magnets in the rotor in the application demonstration later in this paper. This was the main driving force behind testing the feasibility of using resin infiltration to realize consolidation and structural integrity of the printed magnets. A representative cross-section of an infiltrated is presented in FIGURE 4 (b) where the green regions denote the infiltrated EpoFix resin system with the EpoDye as observed using the optical microscope under the

TABLE 3. Comparison of the mechanical and magnetic properties of the as-built and resin infiltrated Nd-Fe-B magnets produced using PBF-LB and the conventional magnets.

	Anisotropy	Compressive strength (MPa)	B_r (T)	H_c (kA/m)	H_{ci} (kA/m)	$(BH)_{max}$ (kJ/m ³)	Metallic density	Powder composition	Ref.
As-built		105.8±2.3	0.65	346	603	62	91%	Nd _{7.5} Pr _{0.7} Zr ₂ ₆ Ti _{2.5} Co _{2.5} Fe ₇₅ B _{8.8} (MQP-S)	This work
Resin infiltrated		325.8±8.6	0.65	343	637	62.8			
Conventional bonded	Isotropic	95 [20]	0.36	-	720	22	80%	5µm MQFP-12-5 (Nd _{17.2} Pr _{0.3} Fe _{75.1} Ce _{6.4} B _{1.0}) and 50 µm MQP-S (Nd _{7.5} Pr _{0.7} Zr _{2.6} Ti _{2.5} Co _{2.5} Fe ₇₅ B _{8.8})	[22]
Conventional sintered	Anisotropic	780 [21]	1.33	-	1480	356	99.9%	Nd _{28.25} Dy _{2.75} Fe _{67.67} Al _{0.15} Ga _{0.1} Nb _{0.1} B _{0.98}	[23]

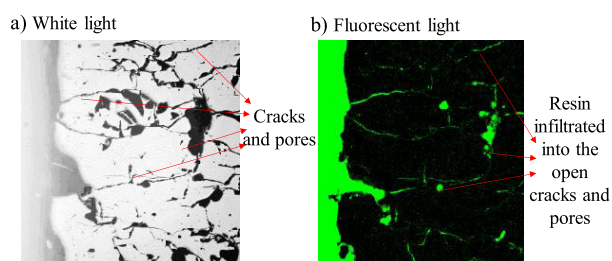


FIGURE 4. a) Optical micrograph under the white light showed the cracks and pores which would weaken the performance of the magnet in the application; b) open cracks and pores were infiltrated and bonded by the resin.

fluorescent light. Visual inspection of the samples at the microscopic level confirmed that the samples were bonded by the resin that infiltrated through the open cracks and pores because of the low viscosity of the resin system and the vacuum environment.

Cylindrical samples of 10 mm diameter and 10 mm height were produced to test the magnetic properties of the samples with and without post-process resin infiltration. The magnetic properties were tested using the Steingroever GmbH-Permagraph test system (Magnik-Physik, Germany) after magnetization in a 2T external magnetic field. To assess the structural integrity of the printed magnets, cylindrical samples of 13 mm diameter and 26 mm height were produced for uniaxial quasistatic compression tests. The tests were conducted using an Instron 5581 universal testing machine equipped with a 50 kN load cell following the ASTM E9-19 Standard [19]. The crosshead speed was set to 0.078 mm/min, resulting in a strain rate of $5 \times 10^{-5} s^{-1}$. The strain data was collected using two linear variable displacement transducers (LVDT). The test was stopped when the sample fractured.

The mechanical properties of the as-built and resin-infiltrated samples are listed in Table 3. The compression tests revealed that the average compressive strength of the resin infiltrated samples (325.8 MPa) was nearly threefold that of the as-built samples (105.8 MPa). Nevertheless, the compressive behavior of the magnets produced in this study in either condition surpassed that of conventional bonded magnets (95 MPa [20]). Although the compressive strength was still relatively low compared to conventional sintered Nd-Fe-B (780 MPa [21]), the positive effect of the low temperature infiltration method is still a significant improvement for this application. Compared to post-process heat-treatment, the resin infiltration process is a low-temperature technique that avoids problems from high temperature post processing. It aids in expanding the range of applications where these parts can be used without the drawback associated with high temperature post processing, in terms of the effect on the microstructure and consequent magnetic properties. Table 3 also lists the magnetic properties of the magnets produced in this study, with and without resin infiltration. The intrinsic coercivity H_{ci} is the resistance of a magnet to demagnetization, the remanence B_r is the residual induction, and the maximum energy product $(BH)_{max}$ denotes the maximum amount of magnetic energy stored in the permanent magnetic material. The magnetic properties of the resin infiltrated samples were comparable to the as-built samples, whereas both were higher than the conventional isotropic bonded magnets. This is attributed to the higher metallic density in the samples produced by PBF-LB. However, the presence of the polymeric resin in the infiltrated magnets limits their thermal bearing capacity, similar to the case of traditional bonded magnets [2]. Although metal infiltration and conventional metallic heat-treatments are common as methods to enhance mechanical properties of PBF-LB parts, i.e. the structural

integrity, of magnets [24], [25], [26], [27], [28], [29], [30], [31], [32], [33], [34], [35], the high temperature involved influences their microstructure and magnetic properties [26], [27], [30], [31], [34], [35], [36], [37]. Resin infiltration is also a low cost method compared to metal infiltration [29], [32] using low melting temperature alloys rich in the rare-earth element. Compared to the sintered Nd-Fe-B magnets, the composition of the PBF-LB material requires significantly less rare earth element (Nd); this is due to the rapid solidification speed during processing and the resultant nanocomposite microstructure [38].

Considering the above aspects, it can be concluded that resin infiltration is more suitable at the current stage to enhance the structural integrity of the originally crack-rich and porous PBF-LB Nd-Fe-B and consequently the capabilities of real applications in the motor during assembly and operation.

IV. ANALYZING AND TESTING THE PBF-LB ND-FE-B MAGNETS IN THE PMA SYNREL MACHINE

A. ANALYSIS USING THE FINITE ELEMENT METHOD

Finite Element Analysis (FEA) was conducted using commercial electromagnetics software, Ansys Maxwell 2D, to assess the performance of the SynRel motor with and without permanent magnets. Different parts of the motor are depicted with arrows in FIGURE 5(a). SynRel and PMA SynRel machines were analyzed with FEA using the obtained magnetic properties of the permanent magnets from the previous tests to obtain their electromechanical performance. Due to the periodic nature of the machine (4- poles 24-slots symmetrical winding configuration) only a quarter of the whole machine was analyzed, using planar symmetry boundary conditions. The finite element mesh used in the analysis is shown in FIGURE 5 (b). The resulting magnetic flux density distribution of the PMA SynRel at no-load condition was simulated to show the resulting magnetic flux density distribution. After the initial analysis, current was imposed in the windings to obtain electromagnetic torque. To determine the contribution of the permanent magnets, various operating points were considered and analyzed. The results considering the no-load condition obtained for the PMA SynRel and the resulting magnetic flux density distribution is depicted in

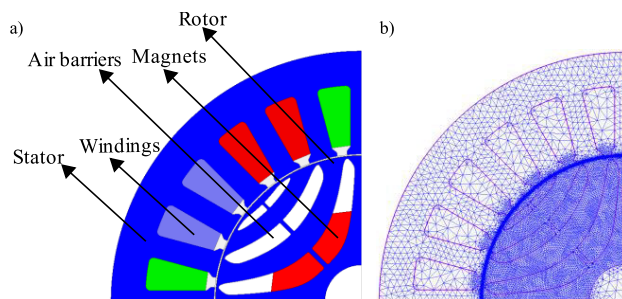


FIGURE 5. Schematic illustration of a) the parts of the PMA SynRel and b) finite element mesh of the PMA SynRel model.

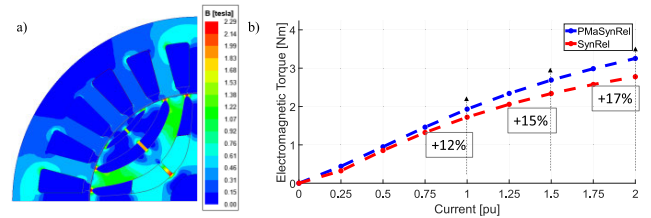


FIGURE 6. a) Magnetic flux density distribution of the PMA SynRel motor at no-load condition; b) Torque versus current characteristics of PMA SynRel and SynRel machines from finite element analysis.

FIGURE 6 (a). The resulting torque of the PMA SynRel and SynRel machines are reported in FIGURE 6 (b).

The electromagnetic torque of the SynRel and PMA SynRel increased with increased current; a considerable improvement of average torque of the PMA SynRel was observed at rated current condition with a 12% increment; this is due to the torque generation mechanism with the assistance of the permanent magnets. The torque improvement increases as the current increases; indeed, at double the rated current becomes 17%. It is important to note that only the inner slots of the air barriers of the rotor were populated by the permanent magnets in this study. Introducing more permanent magnets to a SynRel could obviously yield to a higher improvement in terms of torque and power.

B. DEMAGNETIZATION ANALYSIS

During the operation of an electrical machine, the permanent magnet can be demagnetized if there is a magnetic field that acts against the magnetic flux of the permanent magnets. When it occurs, the magnetic properties of the permanent magnets are permanently reduced thus leading to a loss of performance of the machine. Key dominant factors affecting the resistivity against demagnetization are coercivity and temperature. With the increasing temperature both the remanent flux density of the magnet and the coercivity decreases for Neodymium type magnets. BH curves of the permanent magnet at 20°C, 50°C and 100°C are shown in Figure 7. The demagnetization study is conducted by considering both different temperatures and operating conditions. The first operation is the nominal operation at 25 A_{peak} current amplitude and 60° phase advance angle corresponding to maximum torque per ampere (MTPA) point; the second one is the case where the phase advance angle is 90°. The latter is a much worse case that might happen during a short-circuit when the magnetic field produced by the stator is counteracting on the permanent magnets or in deep flux weakening operating condition.

The following key performance index is considered to evaluate the average demagnetization severity over the magnet area:

$$\begin{aligned}
 & \text{KPIDemag} \\
 &= \left(\left(\frac{\int_{\text{MagnetArea}} S_{\text{Demagd}}(\text{MagnetArea})}{\text{MagnetArea}} \right) - 1 \right) \times 100
 \end{aligned}$$

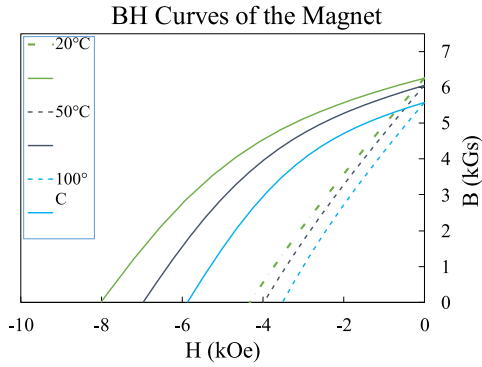


FIGURE 7. BH curves of the magnet at different temperatures.

where the *SDemag* is the severity of the demagnetization between 0 and 1. *SDemag* is the ratio of recoil remanent flux density to the reference remanent flux density. When *SDemag* is 0, magnet is completely demagnetized, and recoil remanent flux density equals to 0. Conversely when *SDemag* is 1, there is no demagnetization. In general, definition of *KPIDemag* naturally makes it in a scale from 0 to 100 and 0 indicates there is absolutely no demagnetization. Results of the demagnetization analysis are presented in TABLE 1 for different cases. Upon investigation, magnets are going through a negligible amount of demagnetization up to 100°C. To further elaborate on the demagnetization performance *SDemag* is shown on the magnets in the FIGURE 8. It is worth noting that most of the demagnetization occurs on the lower left and lower right corner of the magnets due to the presence of sharp corners in the FEM model. It can be inferred that permanent magnets will experience a negligible demagnetization during the normal operation of the electrical machine.

C. MANUFACTURING AND TEST

Once the design and analysis stages were completed, the PMASynRel prototype was manufactured. Two sets of magnets, as-built and resin-infiltrated conditions were inserted into the laminated rotors. The surfaces of the magnets started fragmenting during the insertion into the rotor. The brittle nature of this material and the prior knowledge of its cracking behavior indicated the necessity for post-process treatments to improve the structural integrity of the samples. After the magnets, the motor prototype was installed on an instrumented test rig shown in FIGURE 9 (a) and connected with a load motor (as shown in FIGURE 9 (a)) via a mechanical coupling. The prototype motor was rotated by the load motor at constant speed (1000 RPM). The induced voltage at no load condition, i.e. without current in the windings, was captured and saved using an oscilloscope (Agilent Technologies, MSO-X-2024A, USA) as displayed in FIGURE 9 (b). The prototype motor with the inserted magnets, as-built and resin-infiltrated, were tested individually and the induced voltages were compared with the results obtained from the FEA. The

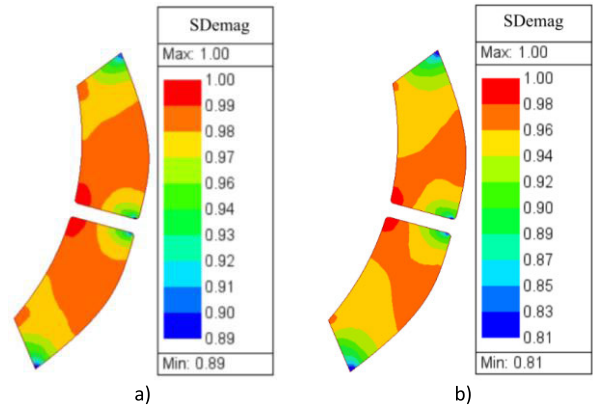


FIGURE 8. Demagnetization maps showing severity of the demagnetization at 25A_{peak} current amplitude and 90° phase advance angle at: a) 20°C b) 100°C.

TABLE 4. Results of demagnetization analysis.

25A _{peak} 50° Phase Advance Angle			
Index	Temperature		
	20°C	50°C	100°C
KPI Demag : Magnet 1 [%]	2.13	3.05	4.01
KPI Demag : Magnet 2 [%]	2.11	3.03	3.98
25A _{peak} 90° Phase Advance Angle			
KPI Demag : Magnet 1 [%]	2.34	3.4	4.69
KPI Demag : Magnet 2 [%]	2.31	3.37	4.64

root mean square (RMS) of the voltages at no-load condition of the machines from FEA and experiments of the two prototypes (as-built and with resin infiltration) are shown in FIGURE 10 and Table.

As presented in Table, the induced no-load voltage of the PMASynRel machine with the as-built permanent magnets was significantly lower than the expected FE values with a reduction of 41.5% in terms of RMS value. The large percentage of discrepancy suggests a significant fracture of the PMs during the assembly process.

In the other hand, the machine prototype equipped with the resin infiltrated permanent magnets shows a much lower the reduction of the induced voltage (12%).

Indeed, the propagation of the cracks and part fracture during the assembly process were minimized due to the bonding effect of the resin within the resin infiltrated parts, supported by the enhanced mechanical properties of the resin infiltrated samples (Table 3).

Figure 10 (b) reports the spectrum of the FE and measured induced voltages. It can be clearly seen that in terms of first harmonic, the experimental results obtained with the resin infiltrated PM are very closed to the FE

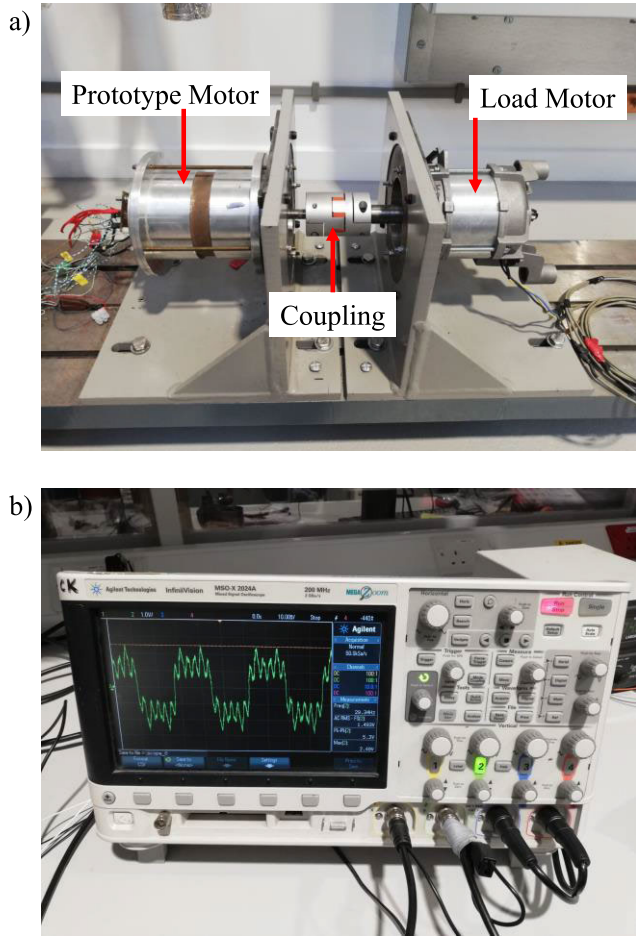


FIGURE 9. a) Test rig of the prototype PMASynRel machine; b) No-load induced voltage of the PMASynRel prototype machine.

TABLE 5. Comparison of the FEA analysis and experiment results.

	FEA	Experiment	
		As-built PM	Resin infiltrated PM
RMS Value [V]	19.5	11.4	17.1
Difference [%]	-	-41.5	-12.5

prediction, being the reduction less than 1V, i.e. less than 5%.

V. SUMMARY

This research has demonstrated the capability and effectiveness of fabricating Nd-Fe-B permanent magnets using laser powder bed additive manufacturing to meet the requirements for the application of a PMASynRel machine. The shapes of the Nd-Fe-B magnets produced with conventional manufacturing are usually rectangular or circular due to the difficulty of machining the magnetic material consisting of

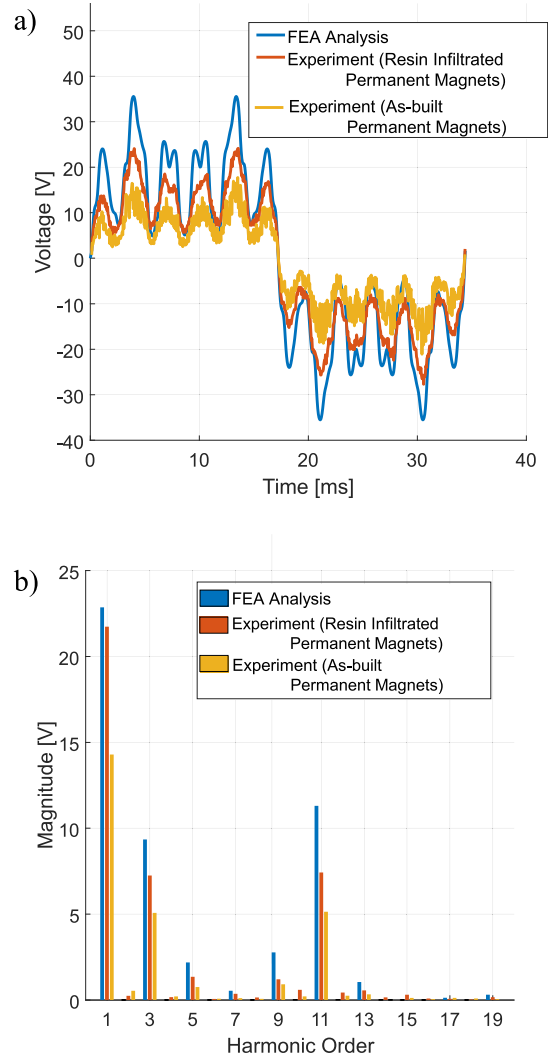


FIGURE 10. Test results: a) voltage waveforms and b) spectrum of the induced voltage.

the predominant brittle intermetallic phase $Nd_2Fe_{14}B$ [47]. Additive manufacturing allowed more complex geometries to be produced without further machining and enabled customized and bespoke designs without the usual cost and time overhead seen in traditional manufacturing. After inserting only one layer of permanent magnets into the air barriers of the rotor in this study, the torque and power produced by the PMASynRel machine improved in the range of 10-15% compared to the SynRel machine without the permanent magnets, as shown in FIGURE 6. In previous studies that investigated the processing of Nd-Fe-B magnets using-PBF-LB, the density of the parts was constrained by the formation of cracks and delamination during the rapid heating and cooling process upon laser irradiation [10], [12], [13]. In addition, defects were significantly observed in the parts with extruded corners due to excessive residual stresses, which weakened the strength of design freedom and structural integrity for the application.

The pores and micro-cracks can act as initiation sites for crack propagation and contribute to low fracture toughness. The low fracture toughness, due to the existence of cracks and pores in this material, diminished the reliability during assembly and operation to meet the requirement of the application. Integrating the findings from the previous study on crack formation in this material [13], it was verified experimentally in this study that the structural integrity of the samples with customized shape was significantly enhanced through scan strategy optimization. Improved temperature management through extensive parameter optimization on this crack-prone material has the potential to further improve the geometric design freedom, relative density, and enhanced magnetic properties. The effectiveness of using PBF-LB to manufacture the permanent magnets for an electrical machine with an optimized geometric design was also successfully demonstrated. Using the optimum combination of parameters and scan strategy, near-net-shape samples can be fabricated within a single build without further machining, which is time and energy effective. Using vacuum resin infiltration as a low-temperature and cost-effective method significantly enhanced the mechanical properties of the samples, whilst maintaining the permanent magnetic properties. The magnetic properties were superior to conventional bonded isotropic magnets owing to a lower volumetric percentage of resin. Compared with metal (e.g. Nd/Pr-rich alloys) infiltration, resin-infiltrated parts cannot bear high temperature (more than 200 °C). Developing a new resin system with a high decomposition temperature, solidification strength and hardness, as well as low viscosity would be beneficial to better support wider applications.

VI. CONCLUSION

Using PBF-LB to additively manufacture Nd-Fe-B permanent magnets with a customized geometry to meet the requirement of the application has been investigated in this study. The findings concluded the following:

1. The capability to produce Nd-Fe-B magnets using PBF-LB has been demonstrated to meet the geometric design requirements for the PMA SynRel machine.
2. The integrity of the parts was affected by the scan strategy as well as the sample's size and geometry. The scan strategy using unidirectional scan tracks in each layer alongside a rotational degree of 90° between the layers yielded the best structural integrity.
3. The brittle nature of the PBF-LB Nd-Fe-B made insertion of the magnets into the motor difficult, where the magnetized fractured parts also magnetically coupled with each other and affected the overall magnetic performance during operation. The trend of the performance of the as-built magnets without post process infiltration agreed with the simulation results. However, defects were introduced in the magnets during magnetization and insertion into the laminated rotor, which resulted in a 41.5% reduction in voltage compared to the simulation results.
4. Resin infiltration was shown to be effective in permeating the open cracks and pores of the magnets, enhancing their mechanical properties during assembly and operation. As a result, the performance of the motor formed by the resin-infiltrated magnets was improved compared to the non-infiltrated magnets, where the difference from the simulation results was reduced to ~12.5%.

ACKNOWLEDGMENT

The author Julan Wu gratefully acknowledges facilities provided by the Centre for Additive Manufacturing (CfAM) and Power Electronics, Machines and Control Group (PEMC) from the University of Nottingham, U.K., associated partner Arnold Magnetic Technologies and funding provided by the INNOVATIVE doctoral programme. The authors would like to thank to Mark Hardy from the Centre for Additive Manufacturing (CfAM), University of Nottingham, U.K.; and Christopher Parmenter from the Nanoscale and Microscale Research Centre (nmRC), University of Nottingham, U.K., for their help with samples preparation and testing.

REFERENCES

- [1] S. Tumanski, "Modern magnetic materials—The review," *Prz Elektrotechniczny*, vol. 86, no. 4, pp. 1–15, 2010.
- [2] D. Brown, B.-M. Ma, and Z. Chen, "Developments in the processing and properties of NdFeB-type permanent magnets," *J. Magn. Magn. Mater.*, vol. 248, no. 3, pp. 432–440, Aug. 2002, doi: [10.1016/s0304-8853\(02\)00334-7](https://doi.org/10.1016/s0304-8853(02)00334-7).
- [3] H. Tiismus, A. Kallaste, T. Vaimann, and A. Rassõlkin, "State of the art of additively manufactured electromagnetic materials for topology optimized electrical machines," *Additive Manuf.*, vol. 55, Jul. 2022, Art. no. 102778, doi: [10.1016/j.addma.2022.102778](https://doi.org/10.1016/j.addma.2022.102778).
- [4] S. Langkau and M. Erdmann, "Environmental impacts of the future supply of rare earths for magnet applications," *J. Ind. Ecology*, vol. 25, no. 4, pp. 1034–1050, Aug. 2021, doi: [10.1111/jiec.13090](https://doi.org/10.1111/jiec.13090).
- [5] M. Murataliyev, M. Degano, M. Di Nardo, N. Bianchi, and C. Gerada, "Synchronous reluctance machines: A comprehensive review and technology comparison," *Proc. IEEE*, vol. 110, no. 3, pp. 382–399, Mar. 2022, doi: [10.1109/JPROC.2022.3145662](https://doi.org/10.1109/JPROC.2022.3145662).
- [6] B. G. Compton, J. W. Kemp, T. V. Novikov, R. C. Pack, C. I. Nlebedim, C. E. Duty, O. Rios, and M. P. Paranthaman, "Direct-write 3D printing of NdFeB bonded magnets," *Mater. Manuf. Processes*, vol. 33, no. 1, pp. 109–113, Jan. 2018, doi: [10.1080/10426914.2016.1221097](https://doi.org/10.1080/10426914.2016.1221097).
- [7] L. Li, A. Tirado, B. S. Conner, M. Chi, A. M. Elliott, O. Rios, H. Zhou, and M. P. Paranthaman, "A novel method combining additive manufacturing and alloy infiltration for NdFeB bonded magnet fabrication," *J. Magn. Magn. Mater.*, vol. 438, pp. 163–167, Sep. 2017, doi: [10.1016/j.jmmm.2017.04.066](https://doi.org/10.1016/j.jmmm.2017.04.066).
- [8] L. Li, A. Tirado, I. C. Nlebedim, O. Rios, B. Post, V. Kunc, R. R. Lowden, E. Lara-Curzio, R. Fredette, J. Ormerod, T. A. Lograsso, and M. P. Paranthaman, "Big area additive manufacturing of high performance bonded NdFeB magnets," *Sci. Rep.*, vol. 6, no. 1, pp. 1–7, Oct. 2016, doi: [10.1038/srep36212](https://doi.org/10.1038/srep36212).
- [9] M. P. Paranthaman, N. Sridharan, F. A. List, S. S. Babu, R. R. Dehoff, and S. Constantinides, "Additive manufacturing of near-net shaped permanent magnets," Oak Ridge Nat. Lab., Oak Ridge, TN, USA, Tech. Rep., ORNL/TM-20, 2016, doi: [10.2172/1311265](https://doi.org/10.2172/1311265).
- [10] J. Jacimovic, F. Binda, L. G. Herrmann, F. Greuter, J. Genta, M. Calvo, T. Tomse, and R. A. Simon, "Net shape 3D printed NdFeB permanent magnet," *Adv. Eng. Mater.*, vol. 19, no. 8, Aug. 2017, Art. no. 1700098, doi: [10.1002/adem.201700098](https://doi.org/10.1002/adem.201700098).

- [11] F. Bittner, J. Thielsch, and W.-G. Drossel, "Microstructure and magnetic properties of Nd-Fe-B permanent magnets produced by laser powder bed fusion," *Scripta Mater.*, vol. 201, Aug. 2021, Art. no. 113921, doi: 10.1016/j.scriptamat.2021.113921.
- [12] F. Bittner, J. Thielsch, and W.-G. Drossel, "Laser powder bed fusion of Nd-Fe-B permanent magnets," *Prog. Additive Manuf.*, vol. 5, no. 1, pp. 3–9, Mar. 2020, doi: 10.1007/s40964-020-00117-7.
- [13] J. Wu, N. T. Aboulkhair, M. Degano, I. Ashcroft, and R. J. M. Hague, "Process-structure-property relationships in laser powder bed fusion of permanent magnetic Nd-Fe-B," *Mater. Des.*, vol. 209, Nov. 2021, Art. no. 109992, doi: 10.1016/j.matdes.2021.109992.
- [14] N. Hopkinson and R. J. M. Hague, *Rapid Manufacturing*. Chichester, U.K.: Wiley, 2005.
- [15] T. Kolb, F. Huber, B. Akbulut, C. Donocik, N. Urban, D. Maurer, and J. Franke, "Laser beam melting of NdFeB for the production of rare-Earth magnets," in *Proc. 6th Int. Electric Drives Production Conf.*, 2016, pp. 34–40, doi: 10.1109/EDPC.2016.7851311.
- [16] E. Carraro, M. Degano, M. Morandini, and N. Bianchi, "PM synchronous machine comparison for light electric vehicles," in *Proc. IEEE Int. Electric Vehicle Conf. (IEVC)*, Dec. 2014, pp. 1–8.
- [17] F. Uberti, L. Frosini, and L. Szabó, "A new design procedure for rotor laminations of synchronous reluctance machines with fluid shaped barriers," *Electronics*, vol. 11, no. 1, p. 134, 2022, doi: 10.3390/electronics11010134.
- [18] Magnequech. (2016). *MQP-S-11-9 Material Safety Data Sheet*. [Online]. Available: <https://mqtechnology.com/product/mqp-s-11-9-20001/>
- [19] *Standard Test Methods of Compression Testing of Metallic Materials at Room Temperature*, Standard ASTM-E9-89a, Annu. B ASTM Standard, 1996.
- [20] W. Xi, W. Liu, R. Hu, Y. Yin, and M. Yue, "Property enhancement of bonded Nd-Fe-B magnets by composite adhesive design," *Mater. Des.*, vol. 192, Jul. 2020, Art. no. 108767, doi: 10.1016/j.matdes.2020.108767.
- [21] (2021). *Characteristics of NdFeB Magnets*. E-Magnets U.K. Accessed: Mar. 16, 2021. [Online]. Available: <https://e-magnetsuk.com/introduction-to-neodymium-magnets/characteristics-of-ndfeb-magnets/>
- [22] T.-S. Yang, N. Wang, and D. P. Arnold, "Fabrication and characterization of parylene-bonded Nd-Fe-B powder micromagnets," *J. Appl. Phys.*, vol. 109, no. 7, pp. 3–10, Apr. 2011, doi: 10.1063/1.3566001.
- [23] X. G. Cui, C. Y. Cui, X. N. Cheng, X. J. Xu, T. Y. Ma, M. Yan, and C. Wang, "Effects of alignment on the magnetic and mechanical properties of sintered Nd-Fe-B magnets," *J. Alloys Compounds*, vol. 563, pp. 161–164, Jun. 2013, doi: 10.1016/j.jallcom.2013.02.093.
- [24] S. Liu and Y. C. Shin, "Additive manufacturing of Ti₆Al₄V alloy: A review," *Mater. Des.*, vol. 164, Feb. 2019, Art. no. 107552, doi: 10.1016/j.matdes.2018.107552.
- [25] N. T. Aboulkhair, I. Maskery, C. Tuck, I. Ashcroft, and N. M. Everitt, "Improving the fatigue behaviour of a selectively laser melted aluminium alloy: Influence of heat treatment and surface quality," *Mater. Des.*, vol. 104, pp. 174–182, Aug. 2016, doi: 10.1016/j.matdes.2016.05.041.
- [26] W. F. Li, T. Ohkubo, and K. Hono, "Effect of post-sinter annealing on the coercivity and microstructure of Nd-Fe-B permanent magnets," *Acta Mater.*, vol. 57, no. 5, pp. 1337–1346, Mar. 2009, doi: 10.1016/j.actamat.2008.11.019.
- [27] H. Sepehri-Amin, Y. Une, T. Ohkubo, K. Hono, and M. Sagawa, "Microstructure of fine-grained Nd-Fe-B sintered magnets with high coercivity," *Scripta Mater.*, vol. 65, no. 5, pp. 396–399, Sep. 2011, doi: 10.1016/j.scriptamat.2011.05.006.
- [28] D. A. Lesyk, S. Martinez, B. N. Mordyuk, V. V. Dzhemelinskiy, D. Lamikiz, and G. I. Prokopenko, "Post-processing of the inconel 718 alloy parts fabricated by selective laser melting: Effects of mechanical surface treatments on surface topography, porosity, hardness and residual stress," *Surf. Coatings Technol.*, vol. 381, Jan. 2020, Art. no. 125136, doi: 10.1016/j.surfcoat.2019.125136.
- [29] M. P. Behera, T. Dougherty, and S. Singamneni, "Conventional and additive manufacturing with metal matrix composites: A perspective," *Proc. Manuf.*, vol. 30, pp. 159–166, Jan. 2019, doi: 10.1016/j.promfg.2019.02.023.
- [30] X. Liu, X. Wang, L. Liang, P. Zhang, J. Jin, Y. Zhang, T. Ma, and M. Yan, "Rapid coercivity increment of Nd-Fe-B sintered magnets by Dy₆₉Ni₃₁ grain boundary restructuring," *J. Magn. Magn. Mater.*, vol. 370, pp. 76–80, Dec. 2014, doi: 10.1016/j.jmmm.2014.06.051.
- [31] D. Salazar, A. Martín-Cid, R. Madugundo, J. M. Barandiaran, and G. C. Hadjipanayis, "Coercivity enhancement in heavy rare Earth-free NdFeB magnets by grain boundary diffusion process," *Appl. Phys. Lett.*, vol. 113, no. 15, Oct. 2018, Art. no. 152402, doi: 10.1063/1.5043389.
- [32] J. G. Zhou, M. Kokkengada, Z. He, Y. S. Kim, and A. A. Tseng, "Low temperature polymer infiltration for rapid tooling," *Mater. Des.*, vol. 25, no. 2, pp. 145–154, Apr. 2004, doi: 10.1016/j.matdes.2003.09.014.
- [33] J. Chen, S. Sheng, and J. Liu, "Enhancement of mechanical performance of porous metallic parts by resin infiltration and selective laser sintering," *J. Harbin. Inst. Technol.*, vol. 5, p. 140, Feb. 2009.
- [34] K. Y. Kim, D. G. Lee, W. Y. Jeung, and I. K. Kang, "Relationship between the intrinsic coercivity and the phases of Nd-(Dy)-Fe-B sintered magnets," *J. Appl. Phys.*, vol. 69, no. 8, pp. 6052–6054, Apr. 1991, doi: 10.1063/1.347767.
- [35] F. Vial, F. Joly, E. Nevalainen, M. Sagawa, K. Hiraga, and K. T. Park, "Improvement of coercivity of sintered NdFeB permanent magnets by heat treatment," *J. Magn. Magn. Mater.*, vols. 242–245, pp. 1329–1334, Apr. 2002, doi: 10.1016/S0304-8853(01)00967-2.
- [36] T. Zhang, F. Chen, Y. Zheng, H. Wen, L. Zhang, and L. Zhou, "Anisotropic behavior of grain boundary diffusion in hot-deformed Nd-Fe-B magnet," *Scripta Mater.*, vol. 129, pp. 1–5, Mar. 2017, doi: 10.1016/j.scriptamat.2016.10.017.
- [37] Z. Chen, H. Okumura, G. C. Hadjipanayis, and Q. Chen, "Microstructure refinement and magnetic property enhancement of nanocomposite Pr₂Fe₁₄B/ α -Fe magnets by small substitution of M for Fe (M=Cr, Nb, Ti and Zr)," *J. Alloys Compounds*, vol. 327, nos. 1–2, pp. 201–205, Aug. 2001, doi: 10.1016/S0925-8388(01)01418-9.
- [38] J. Wu, N. T. Aboulkhair, S. Robertson, Z. Zhou, P. A. J. Bagot, M. P. Moody, M. Degano, I. Ashcroft, and R. J. M. Hague, "Amorphous-crystalline nanostructured Nd-Fe-B permanent magnets using laser powder bed fusion: Metallurgy and magnetic properties," *Acta Mater.*, vol. 259, Oct. 2023, Art. no. 119239, doi: 10.1016/j.actamat.2023.119239.
- [39] A. Foroozmehr, M. Badrossamay, E. Foroozmehr, and S. Golabi, "Finite element simulation of selective laser melting process considering optical penetration depth of laser in powder bed," *Mater. Des.*, vol. 89, pp. 255–263, Jan. 2016, doi: 10.1016/j.matdes.2015.10.002.
- [40] J. P. Kruth, L. Froyen, J. Van Vaerenbergh, P. Mercelis, M. Rombouts, and B. Lauwers, "Selective laser melting of iron-based powder," *J. Mater. Process. Technol.*, vol. 149, nos. 1–3, pp. 616–622, Jun. 2004, doi: 10.1016/j.jmatprotec.2003.11.051.
- [41] J. L. Bartlett and X. Li, "An overview of residual stresses in metal powder bed fusion," *Additive Manuf.*, vol. 27, pp. 131–149, May 2019, doi: 10.1016/j.addma.2019.02.020.
- [42] B. Mooney, K. I. Kourousis, R. Raghavendra, and D. Agius, "Process phenomena influencing the tensile and anisotropic characteristics of additively manufactured maraging steel," *Mater. Sci. Eng., A*, vol. 745, pp. 115–125, Feb. 2019, doi: 10.1016/j.msea.2018.12.070.
- [43] C. Li, Z. Y. Liu, X. Y. Fang, and Y. B. Guo, "On the simulation scalability of predicting residual stress and distortion in selective laser melting," *J. Manuf. Sci. Eng.*, vol. 140, no. 4, Apr. 2018, Art. no. 041013, doi: 10.1115/1.4038893.
- [44] J. Li, D. Deng, X. Hou, X. Wang, G. Ma, D. Wu, and G. Zhang, "Microstructure and performance optimisation of stainless steel formed by laser additive manufacturing," *Mater. Sci. Technol.*, vol. 32, no. 12, pp. 1223–1230, Aug. 2016, doi: 10.1080/02670836.2015.1114774.
- [45] C. Kittel, *Introduction to Solid State Physics*. 7th ed., New York, NY, USA: Wiley, 1996.
- [46] P. F. Richard, B. Robert, and M. S. Leighton, *The Feynman Lectures on Physics*. Pasadena, CA, USA: California Institute of Technology, 1963.
- [47] J. F. Liu, P. Vora, M. H. Walmer, E. Kottcamp, S. A. Bauser, A. Higgins, and S. Liu, "Microstructure and magnetic properties of sintered NdFeB magnets with improved impact toughness," *J. Appl. Phys.*, vol. 97, no. 10, pp. 1–4, May 2005, doi: 10.1063/1.1847215.



JULAN WU received the Ph.D. degree in additive manufacturing from the University of Nottingham, in March 2023. From 2023 to 2024, she was a Research Fellow with the University of Nottingham. Since 2024, she has been with the Research and Development Group, Cooksongold, working on additive manufacturing of precious metals and their applications. Her research interests include materials testing and characterization, additive manufacturing processes, process-structure-property relationships, magnetic materials, and other functional materials and their applications.



CHRIS GERADA (Senior Member, IEEE) received the Ph.D. degree in numerical modeling of electrical machines from the University of Nottingham, Nottingham, U.K., in 2005. He was a Researcher with the University of Nottingham, on high-performance electrical drives and the design and modeling of electromagnetic actuators for aerospace applications. In 2008, he was appointed as a Lecturer in electrical machines, in 2011, as an Associate Professor, and in 2013, as a Professor with the University of Nottingham. He is currently an Associate Pro-Vice-Chancellor for industrial strategy and impact and a Professor of Electrical Machines. He has secured more than £20M of funding through major industrial, European, and U.K. grants. He has authored more than 350 refereed publications. His principal research interests include electromagnetic energy conversion in electrical machines and drives, focusing mainly on transport electrification. He was awarded a Research Chair from the Royal Academy of Engineering, in 2013. He is the Past Chair of the IEEE IES Electrical Machines Committee. He was an Associate Editor of IEEE TRANSACTIONS ON INDUSTRY APPLICATIONS.



OGUZ KORMAN received the M.Sc. degree in electrical engineering from Istanbul Technical University, Turkey, in 2015, and the Ph.D. degree in electrical machines from the University of Nottingham, U.K., in 2024. He is currently a Research Fellow with the Power Electronics, Machines and Control (PEMC) Research Group, University of Nottingham. His research interest includes modeling and design of high-performance electrical machines.



IAN ASHCROFT is currently a Professor of solid mechanics, a member of the Centre for Additive Manufacturing (CfAM), and the Head of the Department of Mechanical, Materials and Manufacturing, Faculty of Engineering, University of Nottingham. His areas of knowledge encompass static and dynamic loading, design optimization, heat, mass transport, and material microstructure understanding. His current research interests include materials testing and characterization, multi-physics finite element analysis, design for manufacture, and structural and multi-objective optimization.



MAURO DI NARDO (Member, IEEE) received the M.Sc. (Hons.) degree in electrical engineering from the Polytechnic University of Bari, Italy, in 2012, and the Ph.D. degree in electrical machine design from the University of Nottingham, U.K., in 2017. From 2017 to 2019, he was with the AROL S.p.A. leading the research and development team focusing on electrical drive design for mechatronics applications. From 2019 to 2023, he was with the Power Electronics and Machine

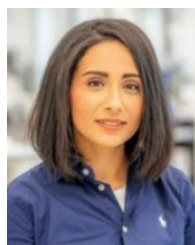


RICHARD J. M. HAGUE is currently a Professor of innovative manufacturing with the Department of Mechanical, Materials and Manufacturing Engineering, University of Nottingham, the Head of the Centre for Additive Manufacturing (CfAM), and the Director of the EPSRC Centre for Innovative Manufacturing in Additive Manufacturing. He has been working in the AM field for 20 years and has a background in leading and managing large multi-disciplinary and multi-partner research projects. His research interests include AM-specific processes, materials, and design/design systems across a wide spectrum of industrial sectors with a particular interest in design/design systems.

Control Group, University of Nottingham, as a Research Fellow. He is currently an Assistant Professor in electrical machines and drives with the Polytechnic University of Bari. He serves as an Associate Editor for IEEE OPEN JOURNAL OF INDUSTRY APPLICATIONS and IEEE TRANSACTIONS ON ENERGY CONVERSION.



MICHELE DEGANO (Senior Member, IEEE) received the master's degree in electrical engineering from the University of Trieste, Trieste, Italy, in 2011, and the Ph.D. degree in industrial engineering from the University of Padua, Padua, Italy, in 2015.



NESMA T. ABULKHAIR received the Ph.D. degree in mechanical engineering from the University of Nottingham. She is currently the Director of the Additive Manufacturing Team, Technology Innovation Institute, Abu Dhabi, United Arab Emirates. She has extensive experience in the field of mechanical engineering, starting with the Ph.D. studies. As an early career researcher, she has an excellent track record of scientific publications (37 articles, H-index 20, and Field Weighted Citation Impact 5.45) and funding (in excess of £2M). Her active research projects span several metal additive manufacturing processes, including powder-based and droplet-on-demand. Her research interests include various metal additive manufacturing processes, with an emphasis on materials processing, manufacturing, and characterization. She serves as the President of the Early Career Researchers Committee for the Association of Industrial Laser Users in the U.K. She is actively engaged in outreach activities to promote awareness about additive manufacturing and has received prestigious awards, including the Anne McLaren Fellowship.

From 2014 to 2016, he was a Research Fellow with the Power Electronics, Machines and Control (PEMC) Research Group, University of Nottingham, U.K., where he was appointed as an Assistant Professor, in 2016, and promoted to an Associate Professor, in 2020, and a Full Professor, in 2023. His main research interests include electrical machines and drives for industrial, automotive, railway, and aerospace applications, ranging from small to large power.

...